ELSEVIER

Catalysis Today 49 (1999) 385–399

CATALYSIS TODAY

Multinuclear MAS NMR studies of zeolites MCM-22 and MCM-49

G.J. Kennedy[a,*], S.L. Lawton[a], A.S. Fung[a], M.K. Rubin[a], S. Steuernagel[b]

[a]*Mobil Technology Company, Paulsboro Technical Center, P.O. Box 480, Paulsboro, NJ 08066-0480, USA*
[b]*Bruker Analytische Messtechnik GMBH, Silberstreifen, D-76287, Rheinstteten, Germany*

Abstract

MCM-22 and MCM-49 comprise a new class of molecular sieves that crystallizes as thin sheets or platelets and has many unusual structural features. MCM-22 is first synthesized hydrothermally as a precursor, MCM-22(P), that condenses upon calcination to a three-dimensional framework (MCM-22). Its framework topology is comprised of two independent pore systems, both accessible through 10-membered rings. One of these pore systems is defined by two-dimensional sinusoidal channels, which maintain an effective 10-ring diameter throughout the structure. The other consists of large supercages whose inner free diameter, 7.1 Å, is defined by 12 rings with inner height of 18.2 Å. MCM-49 has the same framework topology as MCM-22, but is synthesized directly in the reaction gel and therefore still contains the organic template. Multinuclear MAS NMR studies of MCM-22 (P), MCM-22, and MCM-49 are presented and discussed in light of the proposed structure and provide new insights into this novel class of materials. The structural information obtained from this NMR investigation is complementary to and consistent with the structure proposed from X-ray diffraction measurements. ^{13}C NMR data support the existence of different dual pore systems within both MCM-22(P) and MCM-49. ^{27}Al MAS NMR spectra exhibit three distinct T_d resonances that can be interpreted in terms of the proposed framework topology. ^{29}Si MAS studies of a highly siliceous MCM-22 prepared by hydrothermal dealumination confirm the presence of at least one *buried* T-site in its framework structure that is not accessible to a channel wall, favor the orthorhombic form of the proposed structure, and support the presence of the modified dodecasil-1H cage.

1. Introduction

MCM-22 is a novel molecular sieve that crystallizes as thin sheets or platelets, and has an unusual crystal structure [1]. The thin crystals exhibit hexagonal morphology with the unit cell *c*-axis perpendicular to the plate surface. Its framework topology is comprised of two independent pore systems, both accessible through 10-membered rings. One of these pore systems is defined by two-dimensional sinusoidal channels, which maintain an effective 10-ring diameter throughout the structure. The other consists of large supercages whose inner free diameter, 7.1 Å, is defined by 12 rings with a inner height of 18.2 Å.

The MCM-22 structure contains hexagonal sheets constructed by interconnecting $\{4^3 5^6 6^3 [4^3]\}$ cages using shared 4-ring faces in a manner similar to that found in dodecasil-1H (DOH). The $\{4^3 5^6 6^3 [4^3]\}$ cage (Fig. 1B) is a modification of the $[4^3 5^6 6^3]$ cage (Fig. 1A), in which the two tetrahedral T atoms residing on the idealized three-fold axis of the cage join together inside the cage through a shared oxygen

*Corresponding author.

0920-5861/99/$ – see front matter
PII: S0920-5861(98)00444-1

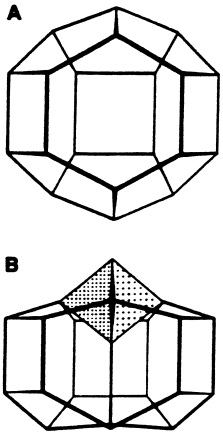

Fig. 1. (A) $[4^3 5^6 6^3]$ cage in dodecasil-1H (B) $\{4^3 5^6 6^3 [4^3]\}$ cage in MCM-22 (from [1]).

atom. This very unusual coordination inside the cage is completed by placement of a TO_3 cap on top of the cage, thereby forming a small $[4^3]$ unit. This $[4^3]$ unit is shown with shading in Fig. 1B. This small unit has previously been found in three zeolites that form the natrolite group, consisting of edingtonite, natrolite and thomsonite. The MCM-22 layer (Fig. 2) contains two sheets of $\{4^3 5^6 6^3 [4^3]\}$ cages. These sheets form the walls of 12-ring pockets on either side of the MCM-22 layer. These sheets are bonded together through double 6 rings that cap the 12-ring pockets and create a 10-ring channel system within the layer. The arrangement of these double 6 rings at the center of the layer creates another new unit that has $[4^2 5^8 10^2]$ topology. The $[4^3]$ caps of the $\{4^3 5^6 6^3 [4^3]\}$ cages are oriented outward from the layer, so that bonding between adjacent

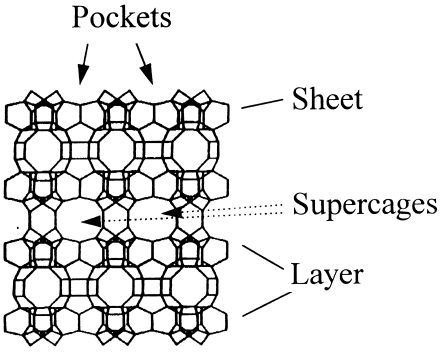

Fig. 2. Model of h0l projection of MCM-22 structure illustrating sheets, layers, supercages, and pockets (from [1]).

MCM-22 layers can occur through these apical atoms, as in the natrolite group of zeolites. The MCM-22 12-ring surface pocket resembles a DOH $[6^8 5^{12}]$ cavity with the 6-ring cap removed from one end. In MCM-22, each pair of opposing 12-ring surface pockets forms a large supercage with $[6^{14} 5^{12} 10^6]$ topology and inside free dimensions of $7.1 \times 7.1 \times 18.2$ Å. Access to the supercages occurs through slightly elliptical 10-ring apertures, created with the $[4^3]$ caps joining the layers together. This two-dimensional interlayer pore system is completely separate from the two-dimensional intralayer system mentioned above, with its slightly tortuous channels accessed by elliptical, folded 10 rings.

The unusual nature of the MCM-22 topology is further underscored by the fact that it can be formed by two very different routes: direct hydrothermal synthesis from a reaction gel or by calcination of a layered precursor. MCM-22 can be made hydrothermally in a reaction mixture with a variety of cyclic amines as a directing agent [2,3]. The two-dimensional layered product, known as MCM-22 precursor or MCM-22(P), is characterized by an X-ray diffraction (XRD) powder pattern with sharp and broad peaks. Upon calcination at 538°C, the precursor undergoes a change in structure to produce a crystalline three-dimensional MCM-22 framework topology material. However, when the mole ratio of the organic cations to inorganic cations is decreased to a value typically less than 2.0, a new material, MCM-49, is formed that exhibits an XRD pattern nearly identical with that for MCM-22 but with subtle, distinct differences in peak positions and intensities [4]. The general similarities in the XRD patterns suggest that the framework topology of MCM-49 may be isostructural with that of MCM-22. When hexamethyleneimine (HMI) is used as the directing agent in a (Si,Al) synthesis, MCM-49 generally has a lower silica/alumina (SiO_2/Al_2O_3) ratio (a range of 17–22) than does MCM-22(P) (21–31). When the concentration of alkali cations in the (Si,Al) reaction mixture (relative to the concentration of HMI) is low, MCM-22 precursor is preferentially formed, a material that must then be calcined to produce the MCM-22 topology. When the relative concentration of alkali cations is high, the MCM-22 topology (MCM-49) is synthesized directly, with the organic cation still present in the pores. Thus, by increasing the relative proportion of

alkali in the reaction gel, formation of MCM-49 is favored, with more aluminum incorporated into its framework than in the MCM-22(P) framework. The pattern of MCM-22(P) is distinctly different from those of MCM-49 and MCM-22. And, although the pattern of MCM-49 appears, at first glance, to be identical with that of MCM-22, subtle differences in peak positions and intensities of the lines serve to classify this material as a distinct member [5]. For a given framework composition, the unit cell *a* parameter is constant (14.26–14.29 Å) whereas the *c* parameter generally is not. The relationships for the average *c* parameters is: MCM-22(P) > MCM-49> MCM-22 (i.e. 26.80 Å > 25.39 Å > 25.16 Å)

Thus, the novelty of the MCM-22/-49 framework is exemplified by

1. the presence of a very unusual T–O–T chain that passes through the center of a modified DOH [$4^3 5^6 6^3$] cage resulting in a framework tetrahedral atom being 'buried' inside the cage,
2. the TO_3 cap that is on the top of the DOH cage,
3. the interlayer linkage through the TO_3 caps are formed both by direct synthesis and by post-synthesis calcination of a two- dimensional precursor, and
4. the average interlayer distances (*c* parameter) are consistently ~0.2 Å longer in [Al]-MCM-49 than in [Al]-MCM-22.

These unusual structural features make this family of materials especially appealing for further characterization studies [5,14–21,34]. In this contribution, we report our high resolution solid state NMR studies of MCM-22(P), MCM-22, and MCM-49 with particular focus on how the NMR data relates to the proposed structures. We also provide evidence that shows a variety of ways in which the proposed model for MCM-22/-49 is consistent with experimental data.

2. Experimental

2.1. Sample preparation

Samples of MCM-22 (P), MCM-22, and MCM-49 were synthesized as previously described [1–5]. The highly siliceous MCM-22 sample in this study was prepared by hydrothermal dealumination as previously described [34]. This MCM-22 sample was studied with ^{29}Si MAS NMR before and after saturation with 2,4-pentanedione and toluene. These samples were prepared at room temperature by dropwise addition of the organic directly to the MCM-22 in the MAS rotor until the samples were visibly saturated. These saturated samples were then left standing at room temperature for 10 min prior to capping the rotors and recording the NMR data.

2.2. NMR procedures

The ^{29}Si MAS NMR spectra were obtained on a Bruker AM-500 spectrometer at 99.35 MHz with 4.5 kHz spinning speeds, 60° excitation pulses, and a 60 s recycle time. Chemical shifts are referenced to TMS. ^{27}Al MAS NMR spectra were obtained at different field strengths (17.6 T, 11.7 T, 9.4 T, and 6.3 T). The 11.7 T spectra were recorded on a Bruker AM-500 NMR spectrometer at 130.31 MHz with 4–6 kHz spinning speeds, 1.0 μs excitation pulses (solution $\pi/2 = 6\,\mu s$), and 0.1 s recycle times. The 9.4 T spectra were obtained on a Bruker MSL-400 NMR spectrometer at 104.26 MHz with 5.00 kHz spinning speed, 1.0 μs excitation pulses (solution $\pi/2 = 6\,\mu s$), and 0.1 s recycle times. The low field (6.3 T) spectra were obtained on Jeol FX-270 NMR spectrometer at 70.3 MHz with a Chemagnetics probe. The 17.6 T spectra were recorded on a Bruker DMX 750 NMR spectrometer at 195.5 MHz, with 14 kHz spinning speeds, 2.0 μs excitation pulses, and 2.0 s recycle delays. The ^{27}Al chemical shifts were referenced to 1 M aqueous solution of $Al(NO_3)_3$ at $\delta = 0.0$ ppm.

^{13}C CP/MAS NMR spectra were obtained on a Bruker MSL-400 NMR spectrometer at 100.61 MHz using a contact time of 1 ms, a 5 s recycle delay, and a spinning rate of 3.1 kHz. The ^{13}C chemical shifts were referenced to TMS using the methine resonance of adamantane ($\delta = 38.3$ ppm from TMS) as a secondary standard. ^{13}C NMR solution spectra of HMI and HMI $- H^+$ were obtained on a Bruker AM-500 spectrometer at 125.76 MHz using a 9.1 μs pulse ($\pi/2$ pulse), composite pulse proton decoupling, and a 4 s recycle delay.

2.3. Temperature programmed base desorption (TPBD) experiments

Temperature Programmed Base Desorption (TPBD) data were collected from 25 to 700°C at a

heating rate of 10°C/min under flowing He, using a duPont 951 thermogravimetric analyzer. The effluent was bubbled continuously through a H_3BO_3/NH_4Cl buffer solution. The pH of the buffer solution was kept constant by automatically titrating with a sulfamic acid solution.

3. Results and discussion

3.1. Influence of HMI on the MCM-22(P), MCM-22, and MCM-49 structures

In the light of the different synthesis routes and *c*-parameters, the role of the organic directing agent (HMI) is of particular interest. MCM-22 contains two void spaces, the interlayer supercages and the intralayer sinusoidal channels. Although the structure of MCM-22(P) is not known, high resolution electron micrographs have revealed that the basic layer of atoms that forms the sinusoidal channels is present (Fig. 2). It is anticipated that MCM-22(P) will also contain some form of interlayer void space, and that both the interlayer and intralayer regions will contain HMI. Since MCM-49 is synthesized directly from the reaction gel, it is expected that this material will also contain HMI in the same regions.

Shown in Fig. 3 are the ^{13}C CP/MAS NMR spectra of MCM-22(P) and MCM-49. The C_1 carbon resonances of hexamethyleneimine (HMI) occur at 49 and 57 ppm and the C_2 and C_3 resonances overlap at 27 ppm. The ratios of the peak areas at 27, 49, and 57 ppm are 4.0 : 1.1 : 0.7 and 4.0 : 1.5 : 0.4 in the MCM-22(P) and MCM-49 spectra, respectively. The ^{13}C NMR chemical shift data are listed in Table 1. The solution chemical shift data for HMI and HMI $\times$ H^+ are included for comparison. Interestingly, each signal is shifted to higher field upon protonation of the HMI. The observation of this protonation-induced upfield shift is consistent with what has been previously reported for various aliphatic amines and *N*-heterocyclic six membered ring compounds [6,7].

It has been shown that the ^{13}C CP/MAS NMR spectra of occluded organic directing agents in synthetic zeolites are sensitive to the geometry of the intracrystalline void space in which they are located [8–12]. For example, the ^{13}C CP/MAS spectra of high silica zeolite A (ZK-4) contain two distinct resonances

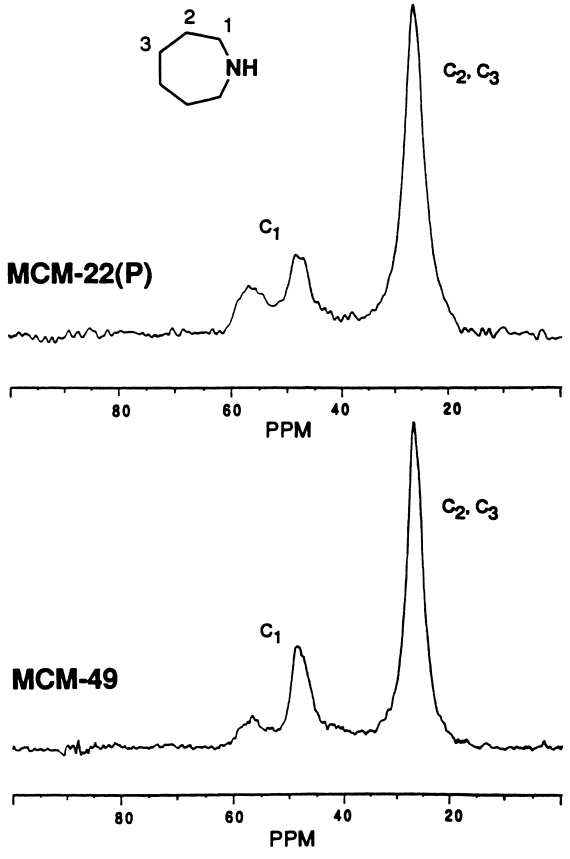

Fig. 3. ^{13}C CP/MAS NMR spectra of MCM-22(P) and as-synthesized MCM-49 (from [5]).

Table 1
^{13}C NMR chemical shifts (ppm from TMS)[a]

Sample	C_1	C_2	C_3
MCM-22(P)[b]	56.8, 48.5	26.7	26.7
MCM-49[b]	56.8, 48.5	26.7	26.7
HMI	48.9	31.0	26.7
HMI − H^+	45.6	26.6	24.9

[a] From [5].
[b] C_2 and C_3 carbon resonances of HMI overlap in MCM-22 and MCM-49.

corresponding to TMA^+ trapped in the α and β cages of the zeolite framework [8]. Interestingly, two resonances are observed for the C_1 of HMI in the ^{13}C spectra of the MCM-22(P) and MCM-49 (Fig. 3). These two C_1 resonances could be due to: (i) decomposition of the HMI, (ii) a mixture of protonated and

non-protonated HMI, and/or (iii) the presence of two distinct void spaces in which the HMI can reside. The ratio of the C_2/C_3 peak area to the C_1 peak area in each sample is close to 2 : 1. Thus, it is unlikely that the second C_1 resonance (57 ppm) is due to decomposed HMI, suggesting that the HMI in both materials is intact. In addition, a comparison of the ^{13}C spectra in Fig. 3 with those of HMI and protonated HMI confirm that the HMI is incorporated intact in the synthesis and that the data indicate that the two C_1 resonances observed in the solids spectra are not simply due to the presence of a mixture of protonated and unprotonated HMI residing in the same environment. In fact, if both species were present, their C_1 resonances should overlap in the 45–49 ppm region of the spectrum. Therefore, the observation of the two resonances for the C_1 of HMI in MCM-22(P) and MCM-49 suggest that the HMI may reside in two distinct environments within these two materials.

The intact incorporation of HMI during the synthesis of MCM-22(P) and MCM-49 is further substantiated by TGA experiments [5]. The weight loss profiles and basic gaseous species desorption curves of the MCM-22(P) and MCM-49 are similar and can be classified into 'low' and 'high' temperature regimes: 200–400°C and 400–500°C, respectively. The base desorption profiles are illustrated in Fig. 4.

In the 'low' temperature regime, two well-defined base desorption peaks were observed in MCM-22(P) with maximum rates of desorption at 232 and 311°C. These desorption peaks were less resolved in MCM-49. Further, a larger amount of base was desorbed in the 'low' temperature regime with MCM-22(P) than with MCM-49, consistent with a higher weight loss (37% versus 30%) observed in the TGA profile of MCM-22(P) than in that of MCM-49. In the 'high' temperature regime, the maximum rate of base desorption occurred at 450–460°C and the amount of base desorbed from MCM-22(P) was similar to that from MCM-49.

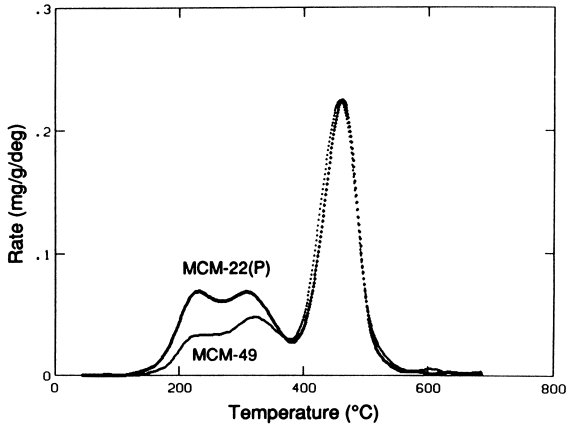

Fig. 4. TPBD profiles of MCM-22(P) and MCM-49 (from [5]).

As the HMI desorption occurred at temperatures higher than the boiling point of HMI (138°C), those desorbed in the 'low' temperature regime were not physisorbed on the external surface of the zeolite crystal. The bimodal weight loss and base desorption profiles observed for as-synthesized MCM-22(P) and MCM-49 suggest that HMI probably resides in two distinct environments, and leads to a difference in the pathway by which HMI is desorbed. This suggestion is consistent with the ^{13}C NMR data.

From the above proposed structure of MCM-22(P), HMI can be located in either the 10-ring channel or the pre-condensed interlayer region. One should expect a difference in the desorption kinetics of HMI from these two distinct locations. The 'high' temperature peak is assigned to the desorption of HMI located in the 10-ring intralayer channel. The appearance of this 'high' temperature peak at 450–460°C may suggest that the HMI is 'trapped' in the 10-ring channel. This 'trapped' HMI can only be removed by decomposing the HMI. This speculation is consistent with the temperature ranges at which the decomposition of adsorbed amines in ZSM-5 occurs [13]. Those HMI species residing in the pre-condensed interlayer region, having pore openings greater than 10 rings, account for the desorption in the 'low' temperature regime.

The HMI distribution among these two void spaces appears to be related to the subtle structural differences between MCM-22(P) and MCM-49. Using the assignment that the desorption temperature regimes correspond to the location of HMI, TPBD and ^{13}C NMR data can provide a more quantitative estimate of the amount of HMI residing in each regime.

The TGA/titration data indicate that the MCM-22(P) and MCM-49 being investigated in this work have similar amounts of HMI located in the 10-ring channel (1.16 versus 1.11 meq/g). However, MCM-22(P) has ~2 times more HMI incorporated in the interlayer region than does MCM-49 (0.84 meq/g in

MCM-22(P) versus 0.46 meq/g in MCM-49). The intensities of the two C_1 resonances in the NMR spectra reflect the HMI population in each of these two environments. The ratio of these two HMI species in the present samples are 0.62 : 1 (MCM-22(P)) and 0.26 : 1 (MCM-49). These results are in good agreement with the TGA data. The NMR data support the hypothesis that the more intense peak (at 48 ppm) is associated with HMI in the 10-ring channel and corresponds to the 'high' temperature desorption peak in the TGA profile. Similarly, the smaller peak (at 57 ppm) is associated with HMI in the interlayer region and corresponds to the 'low' temperature desorption peak.

3.2. *MCM-22 versus MCM-49: the c-parameter puzzle*

Striking similarities in the XRD powder patterns of MCM-22 and MCM-49 indicate that the two framework topologies are probably identical. The fact that the average unit cell *c*-parameter is ~0.2 Å longer in [Al]-MCM-49 than in [Al]-MCM-22 is therefore intriguing. We initially considered the possibility that the presence of HMI in the pores induced an expansion in the *c*-parameter. However, TPBD/XRD studies showed that the thickness of the layers in the MCM-22/-49 framework is not influenced by the presence of HMI in the intralayer pores and the unit cell *c*-parameter of MCM-49 is not significantly altered by removal of HMI from the interlayer region. An alternate explanation, then, may be preferential siting of aluminum in the framework position T_1, a key site in the interlayer bridge. Location of this bridge in the framework structure is depicted in Fig. 5.

Evidence that aluminum siting at T_1 may influence the value of *c* originates with the method of synthesis. Recall that MCM-49 forms in situ in a reaction gel having a much higher alkali concentration than is used to synthesize MCM-22(P). Alkali ions presumably catalyze formation of this bridge and, if so, T_1 may become a primary site for aluminum for charge balance. Since Al–O bonds (1.75 Å in length) are longer than Si–O bonds (1.61 Å in length), the difference, 0.14 Å, may account for the observed difference between the *c*-parameters of MCM-49 and MCM-22. If T_1 is aluminum-rich, there would then have to be sufficient loss of Al from this site during calcination to account for the reduction in *c* to the value observed for MCM-22.

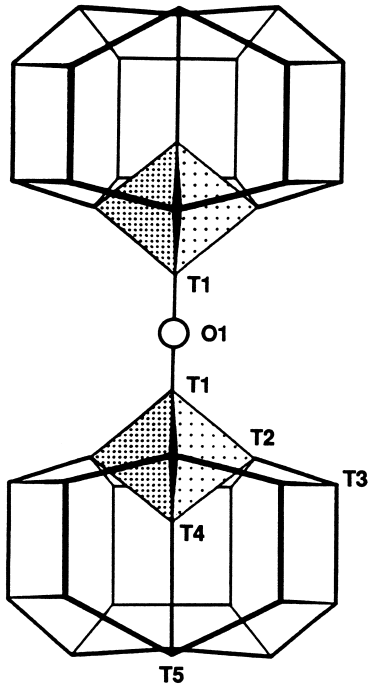

Fig. 5. The interlayer bridge in the MCM-22 framework (from [5]).

The ^{27}Al MAS NMR spectra of framework aluminosilicates usually consist of one tetrahedral (T_d) Al resonance in the 54–68 ppm region of the spectrum that reflects the average environment of an Al atom in the tetrahedral framework [12]. The ^{27}Al MAS NMR spectra of MCM-22 (P) and the as-synthesized MCM-49 are both comprised of two T_d resonances centered at ~50 and ~56 ppm. The calcined forms of both exhibit a third T_d resonance at ~61 ppm (see Figs. 6–8). This peak at 61 ppm is also observed in the very high field (17.6 T) spectra of as-synthesized MCM-49, and as a shoulder in MCM-22(P). Hunger et al. have also reported the observation of three T_d resonances in MCM-22 [14]. The observation of more than one T_d resonance for a zeolite is rare. Prior to this work on MCM-22/-49, zeolites omega [22] and ZSM-18 [23] were the only known cases of zeolites that exhibit two T_d Al resonances. In addition, the uniqueness of the MCM-22/-49 framework is further illustrated by the observation that one of the three T_d Al resonances (at

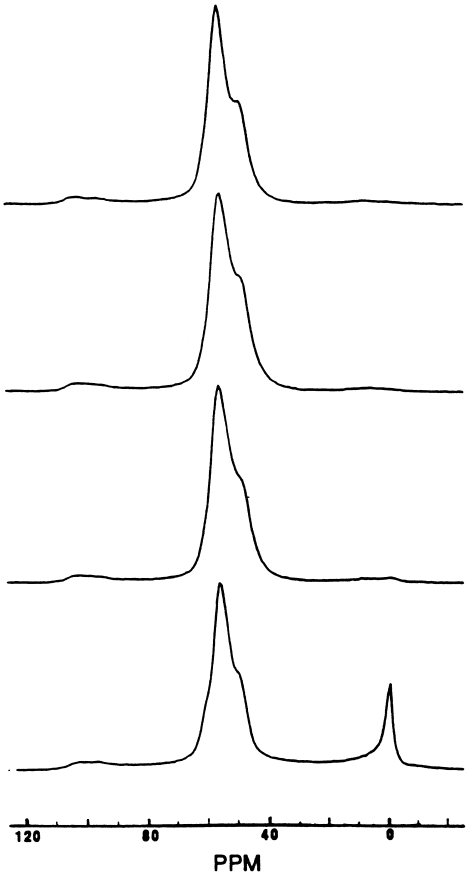

Fig. 6. ^{27}Al MAS NMR data (9.4 T), from top to bottom, of MCM-22(P), after calcination at 592°F/3 h; after calcination at 592°F/6h; and after calcination at 1000°F/16 h (from [5]).

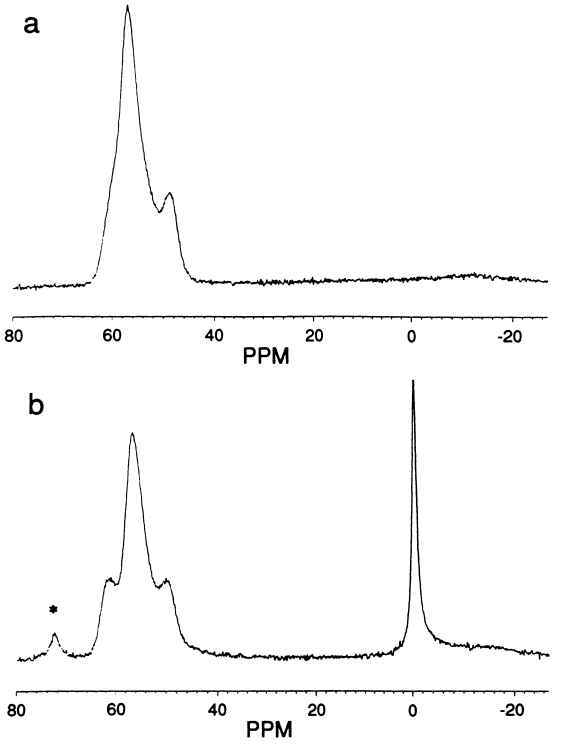

Fig. 7. ^{27}Al MAS NMR spectra (17.6 T) of (a) MCM-22(P) and (b) MCM-22. (from [5]).

$\delta = 50$ ppm) falls *outside* the spectral region that has been ascribed to zeolites.

The origin of the additional T_d Al resonances in MCM-22 and MCM-49 could be due to either a second order quadrupolar interaction or additional T_d Al species (as is the case in omega and ZSM-18). These two possible explanations for the observed spectral features in MCM-22 and MCM-49 were investigated by multiple field and Double Rotation (DOR) NMR experiments [5]. These experiments confirmed that the Al species have small quadrupolar coupling constants and are apparently in highly symmetric environments. These data indicate that no significant second order quadrupolar interactions are present and that the additional T_d Al resonances in MCM-22(P), MCM-22, and MCM-49 are due to distinct T_d Al species.

Shown in Fig. 6 from top to bottom are the 9.4 T ^{27}Al MAS NMR spectra of as-synthesized MCM-22, after calcination at 592°F/3 h, after calcination at 592°F/6 h, and after calcination at 1000°F/16 h. The top three spectra are essentially identical and consist of two T_d Al resonances in the ratio of ∼60:40. Comparison of the spectra of the as-synthesized and calcined MCM-22 show that: (i) ∼15% of the framework Al has come out during calcination to form O_h Al, and (ii) the observation of a third T_d Al resonance at 61 ppm after calcination indicates that structural changes may have occurred in the tetrahedral framework during calcination.

These spectral data are consistent with those reported by others [14–16]. However, these authors did not propose any detailed structural interpretation of their data. What follows is our interpretation of how these unique spectral features relate to the proposed

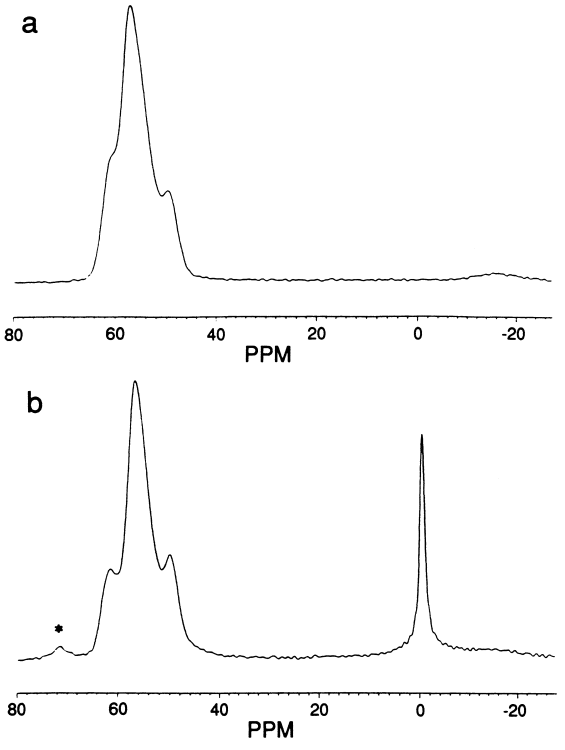

Fig. 8. ^{27}Al MAS NMR spectra (17.6 T) of (a) as-synthesized MCM-49 and (b) MCM-49 (from [5]).

structures. As discussed above, the multiple Al species observed in the NMR spectra are likely due to inherent structural components. In fact, experiments at very high magnetic field (17.6 T) unambiguously confirm the presence of a third T_d peak in MCM-22 (Fig. 7). The increased spectral dispersion and resolution at this field also makes the determination of the relative peak areas straightforward. The spectrum of MCM-22 in Fig. 7 can be simulated in terms of three overlapping gaussian peaks at 61, 56, and 50 ppm in the ratio of 15:62:23. Lippmaa et al. [24] showed that the isotropic chemical shifts of tetrahedral Al correlate well with average Al–O–Si angles in zeolite frameworks. This correlation predicts average angles of 142°, 152°, and 164° for the 61, 56, and 50 ppm components, respectively. Interestingly, the average T–O–T angles in the hexagonal model of the MCM-22 structure range from 143.0 to 161.5. Considering the empirical nature of the bond angle–chemical shift correlation, there is good agreement between the predicted and experimental data. Thus, the experimental ^{27}Al MAS NMR spectrum of calcined MCM-22 is consistent with its unique and unusual framework topology. This comparison of the predicted and experimental data suggests that the experimental spectrum can be tentatively assigned as in Table 2.

Table 2
Tentative assignment of ^{27}Al MAS NMR spectra[a]

Observed chemical shift	Assignment
61	T_2
56	T_1, T_3, T_4, T_5, T_8
50	T_6, T_7

[a] From [5].

Comparison of the ^{27}Al MAS spectra of MCM-22 and MCM-49 reveals some subtle yet interesting differences. Shown in Fig. 8 are the 17.6 T ^{27}Al MAS NMR spectra of MCM-49 before and after calcination at 1000°F/16 h. Comparison of the spectra of as-synthesized MCM-49 with MCM-22(P) shows that the 61 ppm resonance is clearly detected in the as-synthesized MCM-49 but is absent from MCM-22(P). In the case of MCM-22 this peak only becomes apparent upon calcination and condensation of the layers. The observed 61 ppm resonance in the as-synthesized MCM-49 is further evidence for the condensed nature of the layers in this material relative to MCM-22(P). Complete removal of the hexamethyleneimine by high temperature calcination results in an ^{27}Al MAS NMR spectrum that is similar to that of fully calcined MCM-22, with three peaks of relative area 13 : 64 : 23.

Another interesting aspect of the ^{27}Al MAS spectra in Figs. 7 and 8 for MCM-22(P) and MCM-22 is that the observed presence of the resonance at 61 ppm indicates that condensation of the framework (i.e. formation of interlayer T_1–O–T_1 linkages) causes large enough changes in the average T_2–O–T_n angles (where $n = 1$, 3, 3, and 4) to shift the T_2 resonances. Since the changes in the T_d region of the spectrum are due to the combination of framework dealumination and structural changes due to condensation of the layers, it is not possible to determine if Al is preferentially coming from one site during calcination. However, since the observed intensity of the 56 ppm peak is ~20% higher than expected for a random Al distribution it is tempting to infer that it might be indicative of preferential Al siting in T_1.

However, an important conclusion that can be drawn from these data is that high temperature calcination to remove all the hexamethyleneimine results in spectral changes that are consistent with the three dimensional framework of calcined MCM-22. Although the exact nature of these calcination induced changes is unclear, the spectra of the calcined MCM-22 and MCM-49 reflect the structural similarity of these two materials.

3.3. *The buried T-site and TO_3 cap in the modified DOH cage*

^{29}Si MAS NMR experiments on highly siliceous MCM-22 are of fundamental interest because they can provide complementary structural information to that determined by diffraction techniques. Of particular relevance and importance in the characterization of this new framework material is the direct determination of subtle structural features with NMR such as local symmetry, the minimum number of independent T sites per unit cell, their relative populations, and the accessibility of these T sites to channel walls. These structural features can be studied in highly siliceous, crystalline samples.

Shown in Fig. 9 are the ^{29}Si MAS NMR spectra of a highly siliceous MCM-22 sample prepared by hydrothermal dealumination and the H^+ form of the corresponding starting material. The spectrum of the parent is comprised of several overlapping resonances arising from the combined effects of crystallographic site inequivalence and the number of nearest neighbor aluminum atoms on the ^{29}Si chemical shifts. The improved resolution in the steamed sample is due to removal of the effect of the distribution of nearest neighbor atoms on the observed chemical shifts. Since the framework T-sites of the steamed sample are now completely occupied by Si, the observed spectrum is now due to crystallographic inequivalent framework atoms. The high level of spectral resolution in the

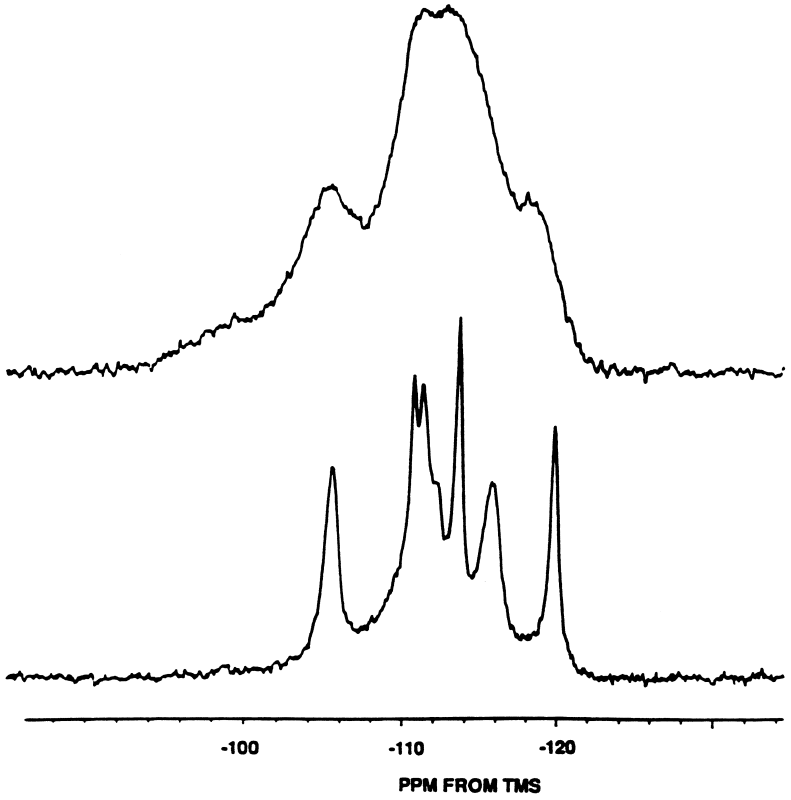

Fig. 9. ^{29}Si MAS NMR spectra of (top) H-MCM-22 and (bottom) highly siliceous MCM-22 (from [34]).

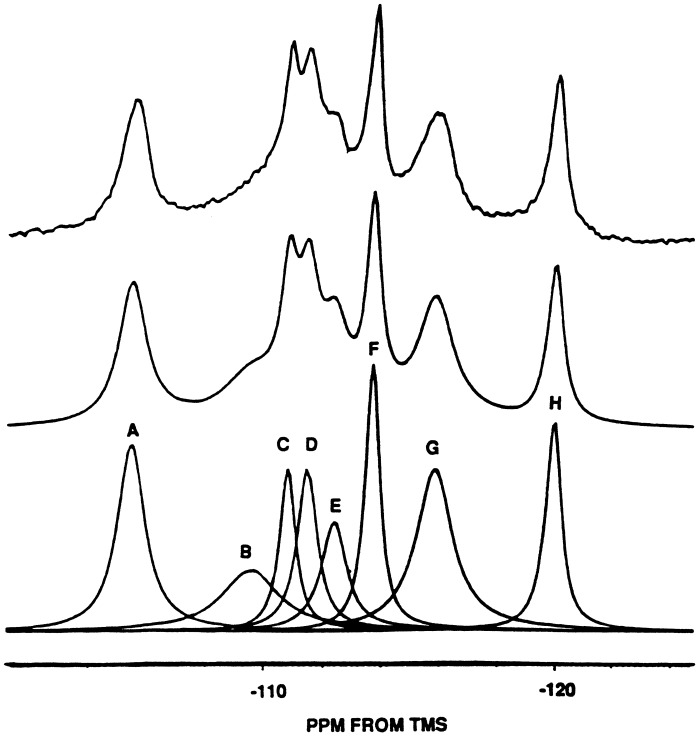

Fig. 10. ^{29}Si MAS NMR spectra of (top) highly siliceous MCM-22, (middle) simulated, and (bottom) components used in simulation. (from [34]).

steamed sample indicates that there are at least seven peaks corresponding to crystallographically distinct T sites. The area under each of these resonances directly relates to the population of the corresponding T site(s). The relative areas of these peaks can be obtained by deconvoluting the experimental spectrum in terms of overlapping Lorentzian lines.

Shown in Fig. 10 from top to bottom are the experimental spectrum, simulated spectrum, and individual peaks used in the simulated spectrum for the siliceous MCM-22. The best fit to the experimental data was obtained by deconvoluting in terms of eight overlapping peaks as shown in the Figure. A broad peak centered at −110 ppm from TMS was included in this simulation in order to fit the experimental data. This peak (labeled B in the Figure) is probably associated with amorphous silica that could be inherent to the starting material and/or formed during the hydrothermal treatment. The other seven peaks correspond to crystallographically distinct T sites within the unit cell of MCM-22. However, the widths of some of the resonances suggest that they may be comprised of other narrower, overlapping resonances.

The spectra in Figs. 9 and 10 indicate that the chemical shift range for MCM-22 is unusually large for a zeolite. For example, the 24 sites in the monoclinic form of ZSM-5 resonate over a chemical shift range of less than 8 ppm (from ∼−109.5 ppm to −117 ppm) [25] and the seven sites in highly siliceous ZSM-12 occur in a chemical shift range of approximately 5 ppm (from ∼−107.9 ppm to −112.9 ppm) [26]. However, as shown in Figs. 9 and 10, the Si nuclei of individual T sites in MCM-22 resonate in a chemical shift range in excess of 15 ppm. This large chemical shift range indicates that an uncharacteristically large distribution of crystallographic environments exists in the MCM-22 structure, further substantiating the novel structure proposed by X-ray diffraction [1].

The spectrum of the highly siliceous sample is a sensitive probe of the unit cell contents at the atomic level and can be directly related to the data from

Table 3
Crystallographic data for framework atoms in MCM-22[a]

Site	Occupancy	Average T–O–T angle
Hexagonal form		
T_1	1	153.8
T_2	3	143.0
T_3	3	150.5
T_4	1	153.8
T_5	1	154.5
T_6	3	161.5
T_7	3	158.5
T_8	3	154.8
Orthorhombic form		
T_1	1	147.5
T_2	1	139.0
T_3	1	148.5
T_4	1	149.5
T_5	2	144.0
T_6	2	142.5
T_7	1	150.0
T_8	1	157.0
T_9	2	152.8
T_{10}	2	151.0
T_{11}	1	162.8
T_{12}	1	149.5
T_{13}	2	143.5

[a] From [34].

X-ray structural determinations. Two space groups were proposed for the structure of MCM-22 [1]. The orthorhombic Cmmm structure is energetically favored over the hexagonal P6/mmm structure. Listed in Table 3 are the individual framework T atoms, their relative occupancies, and average interatomic angles for each of the two models. Thus, in the hexagonal form of the proposed structure of MCM-22 there are eight T sites in the ratio of 1 : 3 : 3 : 1 : 1 : 3 : 3 : 3 and in the orthorhombic form there are 13 T sites in the ratio of 1 : 1 : 1 : 1 : 2 : 2 : 1 : 1 : 2 : 2 : 1 : 1 : 2. The relative areas of the seven resonances (excluding peak B assigned to non-framework silica) are approximately 3 : 2 : 2 : 2 : 3 : 4 : 2. These peak areas are not consistent with the hexagonal space group. In the light of the probability of peak overlap or degeneracies, these observed NMR peak areas for this completely siliceous MCM-22 are consistent with the orthorhombic form of the structure, i.e. (1 + 2) : (1 + 1) : 2 : 2 : (1 + 1 + 1) : (2 + 2) : (1 + 1).

Additional information to help differentiate one space group over the other can be obtained by combining the NMR data with geometric data from the diffraction studies. The differences observed in the chemical shifts reflect differences in the local magnetic environments of the individual silicon atoms. It has been shown that qualitative correlations exist between ^{29}Si chemical shifts and geometric data, such as average T–O–T angles, for zeolites [27–33]. It is important to note that correlations of this type must be used with caution because they are derived from structural parameters that vary over a limited range. Thus, they cannot be used with a high degree of confidence to assign individual ^{29}Si resonances to distinct T sites. However, these correlations can be used in a qualitative way to discriminate between two possible structures, as in the present case of MCM-22. For example, the predicted range of average T–O–T angles (23.3°) obtained from the correlation in reference [32] is in better agreement with the orthorhombic form (range of 23.8°) than with the hexagonal form (range of 18.5°).

^{29}Si MAS NMR spectra of this sample were also obtained using a progressive saturation technique to probe the spin lattice relaxation characteristics of the silicon nuclei [34]. These spin lattice relaxation time experiments provide additional insight and indicate that individual Si nuclei within the MCM-22 framework relax at differing rates. In particular, peak C at −110.8 ppm from TMS relaxes at a significantly slower rate than the other six peaks. The major contribution to the spin lattice relaxation mechanism in highly siliceous zeolitic systems is interactions of the Si nuclei with molecular oxygen [35,36]. Thus, the longer relaxation time observed for peak C suggests that it is associated with Si nuclei occupying a T site that is not on the channel surface (i.e. not in contact with adsorbed oxygen) and is 'buried' inside the three dimensional framework of the MCM-22 structure. This spin lattice relaxation phenomenon was also reported for highly siliceous ZSM-12 [26] and used to assign the resonance associated with the buried T_5 site in ZSM-12. Thus, this observation in MCM-22 confirms that there is a buried T site in the framework and indicates that peak C can be unambiguously assigned to T_3 in the orthorhombic structure or similarly to T_4 in the hexagonal form. Of course, intensity data shows that at least one other T

Table 4
Tentative peak assignments for the ^{29}Si MAS NMR spectrum of highly siliceous MCM-22[a,b]

Peak	Chemical shift	Relative area	Assignment
A	−105.5	3	$T_2 + T_6$
C	−110.8	2	$T_3 + T_1$
D	−111.5	2	T_{13}
E	−112.4	2	T_5
F	−113.7	3	$T_4 + T_7 + T_{12}$
G	−115.8	4	$T_9 + T_{10}$
H	−119.9	2	$T_8 + T_{11}$

[a] Peak assignments are tentative and are based on the observed peak areas, spin lattice relaxation time behavior, and a qualitative correlation.
[b] From [34].

site with a very similar chemical shift contributes to peak C.

Interestingly, the predicted chemical shift for T_3 in the orthorhombic form is −110.6 ppm and for T_4 in the hexagonal form is −113.9 ppm versus the observed experimental value of −110.8. Although, as noted above, it is accepted that these correlations should only be used in a qualitative sense and not to make definitive peak assignments, it is tempting to use this observation as another piece of evidence favoring the orthorhombic form over the hexagonal.

The tentative NMR peak assignments shown in Table 4 for the orthorhombic form of MCM-22 were made on the basis of the observed peak areas, spin lattice relaxation time behavior, and the qualitative relationship between average T–O–T angles and ^{29}Si chemical shifts. These assignments are preliminary and are subject to revision. Two-dimensional NMR experiments to establish Si–O–Si connectivities would provide definitive peak assignments and unambiguous discrimination between the two proposed structures. Experiments of this nature were unsuccessful on this particular sample and a sample exhibiting a higher degree of spectral resolution would be required to make definitive peak assignments. Based on published work on other systems [37–44], the NMR line widths in MCM-22 would have to be a factor of 3 or 4 narrower in order to obtain 2D NMR data.

Subsequent work involving the effects of sorbed organics [45] are consistent with the peak assignments in Table 4. Shown in Fig. 11 are the ^{29}Si MAS NMR spectra of a highly siliceous MCM-22 (A), and this same material after addition of 2,4-pentanedione (B), and toluene (C). These data show that addition of these organics cause very dramatic changes in the corresponding NMR spectra. The observed spectral changes are very specific in nature in that different sorbed molecules cause different and characteristic changes in the spectra. The sharpness of the spectra also indicate no loss of or change in crystallinity. These sorbate induced changes are reversible, the original spectrum (Fig. 11A) being obtained when the organic is removed by calcination.

The observed spectral changes are thought to be due to a modification or a perturbation of the lattice structure of MCM-22 similar to what has been previously reported for ZSM-5 [46–52]. In the case of ZSM-5, addition of varying amounts of different organics to highly siliceous ZSM-5 can induce a monoclinic to orthorhombic phase transition. In the present case of MCM-22, it is postulated that the presence of the organics is not inducing a phase transition, but is rather causing some perturbations of the local geometry at specific T sites in the unit cell while leaving others unaffected.

The individual peak assignments for the spectra shown in Fig. 11 are given in Table 5 for the orthorhombic (Cmmm) form of MCM-22 in which there are thirteen crystallographically distinct T atoms. Close examination of the spectra and the tabulated data indicate that with addition of organic the peaks labeled a, and c remain unchanged, peaks e, g, and h undergo some marginal change in position, and peaks d and f shift by significant amounts. For example, addition of 2,4-pentanedione causes peak d to move from −111.5 to −113.0, resulting in overlap with resonances from peak f that have moved from −113.7 to −113.0. Peak e overlaps with d and f and is now the shoulder at ∼−112.6. Peaks g and h have each moved ∼0.5 ppm upfield.

It is well accepted [26–32] that larger T–O–T angles produce more negative (i.e. upfield) chemical shifts. Thus, the spectral data indicate that the addition of the individual organics cause some average T–O–T angles to get larger and others to get smaller while leaving some essentially unchanged. Interestingly, the unaffected peaks are those that we assigned to the 'buried' T_3 site at −110.8 and the T_1, T_2, and T_6 sites in the [4^3] caps of the modified DOH cages in the orthorhombic form of MCM-22 (Fig. 12). This observation is con-

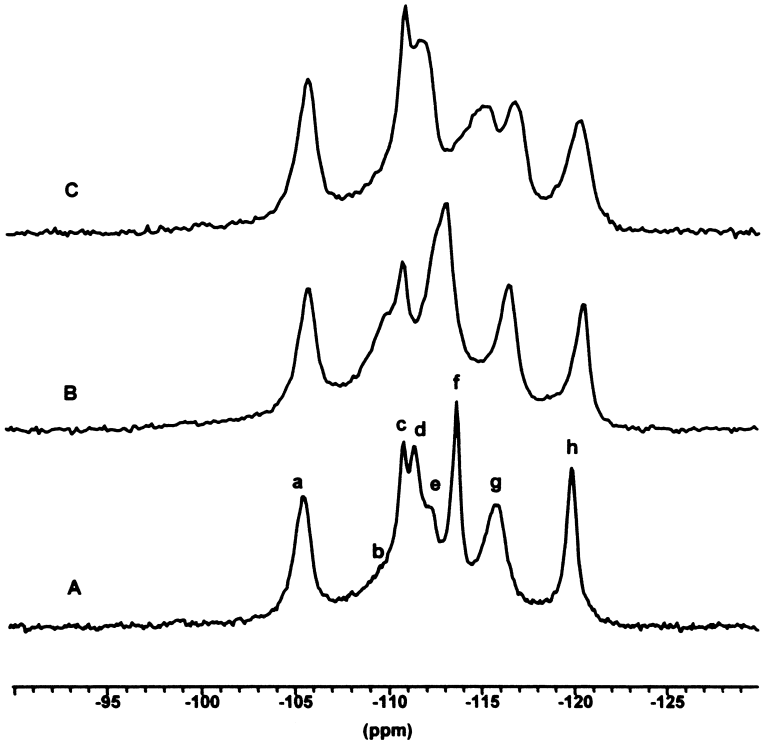

Fig. 11. ^{29}Si MAS NMR spectra of highly siliceous MCM-22 (A), and this same sample after saturation with 2,4-pentanedione (B), and toluene (C) (from [45]).

Table 5
^{29}Si MAS NMR chemical shift[a] data for highly siliceous MCM-22[b]

Peak[c]	Assignment[d]	No organic	2,4-Pentanedione	Toluene
a	$T_2 + T_6$	−105.5	−105.5	−105.5
c	$T_3 + T_1$	−110.8	−110.8	−110.8
d	T_{13}	−111.5	−113.0	−111.8
e	T_5	−112.4	−112.6	−112.0
f	$T_4 + T_7 + T_{12}$	−113.7	−113.0	−113.9 and −115.0
g	$T_9 + T_{10}$	−115.8	−116.3	−116.7
h	$T_8 + T_{11}$	−119.9	−120.3	−120.1

[a] Chemical shifts are ppm from TMS.
[b] From [45].
[c] Broad peak b at −110 ppm from TMS is due to amorphous silica in the sample.
[d] Peaks assigned to orthorhombic (Cmmm) form of MCM-22.

sistent with the expectation that the T_3 site is inaccessible to the sorbates and that the [4^3] cap is quite rigid, thereby providing further evidence for the presence of this unusual modified DOH cage. All the other peaks that experience these sorbate induced changes are in the accessible region of the framework. This suggests that the organic is present in the channels and supercages and that the framework is flexible enough to accommodate local strains induced by the organic without any bond breaking. This again is consistent with the notion that as some average bond angles get larger others have to get smaller. The fact that these

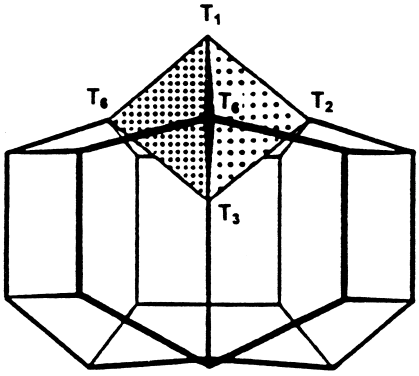

Fig. 12. The modified dodecasil-1H [$4^3 5^6 6^3$] cage with the [4^3] cap (shaded) in MCM-22 (from [45]).

spectral changes reflect local perturbations rather than changes in the crystalline lattice are also evidenced by the reversible nature of these spectral changes.

4. Conclusion

Zeolites MCM-22(P), MCM-22, and MCM-49 have many unusual structural features that are particularly amenable to investigation with NMR techniques. ^{13}C NMR data support the existence of different dual pore systems within both MCM-22(P) and MCM-49. NMR resonances can be assigned to organic directing agent in the sinusoidal intralayer channels and in the precondensed interlayer void spaces. ^{27}Al MAS NMR spectra of MCM-22(P) and MCM-49 exhibit at least two T_d resonances at ~50 and 56 ppm. When these materials are calcined at 1000°F, their spectra clearly show an additional T_d peak at 61 ppm. This observation of three distinct T_d resonances is quite unusual, reflecting the uniqueness of the three dimensional framework, and can be interpreted in terms of the proposed framework topology. Although the exact cause of the longer *c*-parameter in MCM-49 relative to MCM-22 is unclear at this time, it is speculated that it may be associated with the Al distribution in the interlayer region. ^{29}Si MAS NMR characterization of a highly siliceous MCM-22 provide structural information that is complementary to and consistent with the structure proposed from X-ray diffraction measurements and gives further insight into the local geometries of this unique material. The NMR data (i.e. number of peaks, individual peak areas, and chemical shifts) favor the orthorhombic form of the proposed structure. The ^{29}Si MAS NMR data also shows that MCM-22 contains one 'buried' T site in its framework structure that is not accessible to a channel wall and supports the presence of a modified dodecasil-1H cage, as previously proposed from the refinement of the X-ray diffraction data.

Acknowledgements

Helpful interaction and discussion on various aspects of this work with F.C. Kohout, T.F. Degnan, W.J. Roth, C.T. Kresge, J.G. Bendoraitis, L.B. Alemany, C.D. Chang, G.H. Hatzikos, D.N. Lissy, M.E. Leonowicz, J.A. Lawton, J.M. Bennett, A.W. Chester, H.C. Timken, and D.E. Woessner are gratefully acknowledged. Figs. 1 and 2 are reprinted with permission from Science 264, (1994) 1910 (Copyright 1994 American Association for the Advancement of Science). Figs. 3–8 and Tables 1 and 2 are reprinted with permission from J. Phys. Chem., 100 (1996) 3788 (Copyright 1996 American Chemical Society). Figs. 9 and 10 and Tables 3 and 4 are reprinted with permission from J. Amer. Chem. Soc., 116 (1994) 11000 (Copyright 1994 American Chemical Society). Figs. 11 and 12 Table 5 are reprinted from Microporous Materials, 9 209-212, 1997 with kind permission of of Elsevier Science – NL, Sara Burgerhartstraat 25, 1055 KV Amsterdam, The Netherlands. We are grateful to the management of Mobil Technology Company for permission to publish this work.

References

[1] M.E. Leonowicz, J.A. Lawton, S.L. Lawton, M.K. Rubin, Science 264 (1994) 1910.
[2] M.K. Rubin, P. Chu, US Patent 4,954,325 (1990).
[3] C.D. Chang, D.M. Mitko, US Patent 5,173,281 (1992).
[4] J.M. Bennett, C.D. Chang, S.L. Lawton, M.E. Leonowicz, D.N. Lissy, M.K. Rubin, US Patent 5,326,575 (1993).
[5] S.L. Lawton, A.S. Fung, G.J. Kennedy, L.B. Alemany, C.D. Chang, G.H. Hatzikos, D.N. Lissy, M.K. Rubin, H.C. Timken, S. Steuernagel, D.E. Woessner, J. Phys. Chem. 100 (1996) 3788.
[6] J.B. Stothers, Carbon-13 NMR Spectroscopy, Academic Press, New York, 1972, p. 153.
[7] I. Morishima, K. Yoshikawa, K. Okada, T. Yonezawa, K. Goto, J. Am. Chem. Soc. 95 (1973) 165.

[8] R.H. Jarman, M.T. Melchior, J. Chem. Soc., Chem. Commun. (1984) 414.
[9] S. Hayashi, K. Suzuki, S. Shin, K. Hayamizu, O. Yamammoto, Chem. Phys. Lett. 113 (1985) 368.
[10] G. Boxhoorn, R.A. Van Santen, W.A. van Erp, G.R. Huis, D. Clague, J. Chem. Soc., Chem. Commun. (1982) 264.
[11] J.B. Nagy, Z. Gabelica, E.G. Derouane, Zeolites 3 (1983) 43.
[12] G. Engelhardt, D. Michel, High Resolution Solid State NMR of Silicates and Zeolites, Wiley, New York, 1987.
[13] D.J. Parrillo, A.T. Adamo, G.T. Kokotailo, R.J. Gorte, Appl. Catal. 67 (1990) 107.
[14] M. Hunger, S. Ernst, J. Weitkamp, Zeolites 15 (1995) 188.
[15] W. Kolodziejski, C. Zicovich-Wilson, C. Corell, J. Pérez-Pariente, A. Corma, J. Phys. Chem. 99 (1995) 7002.
[16] A. Corma, C. Corell, V. Fornés, W. Kolodziejski, J. Pérez-Pariente, Zeolites 15 (1995) 576.
[17] S. Unverricht, M. Hunger, S. Ernst, H.G. Karge, J. Weitkamp, Zeolites and Related Microporous Materials: State of the Art 1994, Part A; Studies in Surface Science and Catalysis 84, Elsevier, Amsterdam, 1994, p. 37.
[18] A. Corma, C. Corell, J. Pérez-Pariente, Zeolites 15 (1995) 2.
[19] R. Ravishankar, T. Sen, V. Ramaswamy, H.S. Soni, S. Ganapathy, S. Sivasanker, Zeolites and Related Microporous Materials: State of the Art 1994, Part A: Studies in Surface Science and Catalysis 84, Elsevier, Amsterdam, 1994, p. 331.
[20] R. Ravishankar, D. Bhattacharya, N.E. Jacob, S. Sivasanker, Microporous Mat. 4 (1995) 83.
[21] R. Ravishankar, T. Sen, V. Ramaswamy, S. Sivasanker, S. Ganapathy, J. Chem. Soc., Faraday Trans. 91 (1995) 3549.
[22] C.A. Fyfe, G.C. Gobbi, G.J. Kennedy, J.D. Graham, R.S. Ozubko, W.J. Murphy, A.A. Bothner-By, J. Dadok, A.S. Chesnick, Zeolites 5 (1985) 179.
[23] K.D. Schmitt, G.J. Kennedy, Zeolites 14 (1994) 635.
[24] E. Lippmaa, A. Samoson, M. Magi, J. Am. Chem. Soc. 108 (1986) 1730.
[25] C.A. Fyfe, H. Grondey, Y. Feng, G.T. Kokotailo, J. Am. Chem. Soc. 112 (1990) 8812.
[26] C.A. Fyfe, Y. Feng, H. Gies, H. Grondey, G.T. Kokotailo, J. Am. Chem. Soc. 112 (1990) 3264.
[27] J.B. Higgins, D.E. Woessner, EOS 63 (1982) 1139.
[28] J.V. Smith, C.S. Blackwell, Nature 303 (1983) 223.
[29] J.M. Thomas, J. Klinowski, S. Ramdas, B.K. Hunter, D.T.B. Tennakoon, Chem. Phys. Lett. 102 (1982) 158.
[30] S. Ramdas, J. Klinowski, Nature 308 (1984) 521.
[31] G. Engelhardt, R. Radeglia, Chem. Phys. Lett. 108 (1984) 271.
[32] R. Radeglia, G. Engelhardt, Chem. Phys. Lett. 114 (1985) 28.
[33] J.M. Newsam, J. Phys. Chem. 91 (1987) 1259.
[34] G.J. Kennedy, S.L. Lawton, M.K. Rubin, J. Am. Chem. Soc. 116 (1994) 11000.
[35] D.J. Cookson, B.E. Smith, J. Magn. Reson. 63 (1985) 217.
[36] J. Klinowski, T.A. Carpenter, J.M. Thomas, J. Chem. Soc., Chem. Commun. (1986) 956.
[37] C.A. Fyfe, H. Gies, Y. Feng, J. Chem. Soc., Chem Commun. (1989) 1240.
[38] C.A. Fyfe, H. Gies, Y. Feng, J. Am. Chem. Soc. 111 (1989) 7702.
[39] C.A. Fyfe, Y. Feng, H. Gies, H. Grondey, G.T. Kokotailo, J. Am. Chem. Soc. 112 (1990) 3264.
[40] C.A. Fyfe, H. Gies, Y. Feng, H. Grondey, Zeolites 10 (1990) 278.
[41] C.A. Fyfe, H. Gies, Y. Feng, G.T. Kokotailo, Nature 341 (1989) 223.
[42] C.A. Fyfe, H. Grondey, Y. Feng, G.T. Kokotailo, Chem. Phys. Lett. 173 (1990) 211.
[43] C.A. Fyfe, H. Grondey, Y. Feng, G.T. Kokotailo, J. Am. Chem. Soc. 112 (1990) 8812.
[44] C.A. Fyfe, H. Grondey, Y. Feng, G.T. Kokotailo, A. Mar, J. Phys. Chem. 95 (1991) 3747.
[45] G.J. Kennedy, S.L. Lawton, Microporous Mat. 9 (1997) 209.
[46] E.L. Wu, S.L. Lawton, D.H. Olson, A.C. Rohrman, G.T. Kokotailo, J. Phys. Chem. 83 (1979) 2777.
[47] C.A. Fyfe, G.J. Kennedy, C.T. De Schutter, G.T. Kokotailo, J. Chem. Soc., Chem. Commun. (1984) 541.
[48] G.W. West, Aust. J. Chem. 37 (1984) 455.
[49] C.A. Fyfe, G.J. Kennedy, G.T. Kokotailo, J.R. Lyerla, W.W. Fleming, J. Chem. Soc., Chem. Commun. (1985) 740.
[50] D.G. Hay, H. Jaeger, J. Chem. Soc., Chem. Commun. (1984) 1433.
[51] D.G. Hay, H. Jaeger, G.W. West, J. Phys. Chem. 89 (1985) 1070.
[52] C.A. Fyfe, H.J. Strobl, G.T. Kokotailo, G.J. Kennedy, G.E. Barlow, J. Am. Chem. Soc. 110 (1988) 3373.